View metadata, citation and similar papers at core.ac.uk
brought to you by CORE
provided by Catalogo dei prodotti della ricerca

Biomatter 4:1, e955386; January–December 2014; Published with license by Taylor & Francis Group, LLC

Interfacing polymeric scaffolds with primary pancreatic ductal adenocarcinoma cells to develop 3D cancer models

Claudio Ricci[1,2,3], Carlos Mota[3], Stefania Moscato[4], Delfo D'Alessandro[2], Stefano Ugel[1], Silvia Sartoris[1], Vincenzo Bronte[1], Ugo Boggi[5], Daniela Campani[2], Niccola Funel[2], Lorenzo Moroni[3,*], and Serena Danti[2,*]

[1]Department of Pathology and Diagnostics; University of Verona; Verona, Italy; [2]Department of Surgical, Medical, Molecular Pathology and Emergency Medicine; University of Pisa; Pisa, Italy; [3]Tissue Regeneration Department; University of Twente; Enschede, The Netherlands; [4]Department of Clinical and Experimental Medicine; University of Pisa; Pisa, Italy; [5]Department of Translational Research and New Technologies in Medicine and Surgery; University of Pisa; Pisa, Italy

Keywords: cancer, compression molding, electrospinning, emulsion and freeze-drying, metalloproteinase 2 (MMP-2), metalloproteinase 9 (MMP-9), Pancreatic adenocarcinoma, polyethylene oxide terephthalate (PEOT), polyvinyl alcohol (PVA), scaffold

Abbreviations: 2D, Bi-dimensional; 3D, Three-dimensional; BCA, Bicinchoninic acid; BSA, Bovine serum albumin; Dd, double distilled; Ds, double stranded; ECM, Extracellular matrix; G, Gelatin; HRP, Horseradish peroxidase; K-ras, Kirsten rat sarcoma viral oncogene homolog; MMP, Matrix metalloproteinase; PanIN, Pancreatic intraepithelial neoplasia; PBS, Phosphate buffer saline; PCR, Polymer-chain reaction; PDAC, Pancreatic ductal adenocarcinoma; PEOT/PBT, Poly(ethylene oxide terephthalate)/poly(butylene terephthalate); PVA, Poly(vinyl alcohol); Smad4, Mothers against decapentaplegic homolog 4; TME, Tumor microenvironment.

We analyzed the interactions between human primary cells from pancreatic ductal adenocarcinoma (PDAC) and polymeric scaffolds to develop 3D cancer models useful for mimicking the biology of this tumor. Three scaffold types based on two biocompatible polymeric formulations, such as poly(vinyl alcohol)/gelatin (PVA/G) mixture and poly (ethylene oxide terephthalate)/poly(butylene terephthalate) (PEOT/PBT) copolymer, were obtained via different techniques, namely, emulsion and freeze-drying, compression molding followed by salt leaching, and electrospinning. In this way, primary PDAC cells interfaced with different pore topographies, such as sponge-like pores of different shape and size or nanofiber interspaces. The aim of this study was to investigate the influence played by the scaffold architecture over cancerous cell growth and function. In all scaffolds, primary PDAC cells showed good viability and synthesized tumor-specific metalloproteinases (MMPs) such as MMP-2, and MMP-9. However, only sponge-like pores, obtained via emulsion-based and salt leaching-based techniques allowed for an organized cellular aggregation very similar to the native PDAC morphological structure. Differently, these cell clusters were not observed on PEOT/PBT electrospun scaffolds. MMP-2 and MMP-9, as active enzymes, resulted to be increased in PVA/G and PEOT/PBT sponges, respectively. These findings suggested that spongy scaffolds supported the generation of pancreatic tumor models with enhanced aggressiveness. In conclusion, primary PDAC cells showed diverse behaviors while interacting with different scaffold types that can be potentially exploited to create stage-specific pancreatic cancer models likely to provide new knowledge on the modulation and drug susceptibility of MMPs.

Introduction

Pancreatic ductal adenocarcinoma (PDAC) is a malignant neoplasm, estimated to be the fourth cancer killer in the United States and the eighth worldwide.[1] Owing to PDAC minimal symptoms leading to late-stage diagnoses, 75% of patients have dismal prognosis with a 5-year survival rate of only 6%.[1] The remaining 25% of patients are those who undergo surgery for localized diseases, but their 5-year survival rate barely reaches 20%.[2] This malignancy has been associated with several clinical factors responsible for such mortality rates: (i) lack of diagnostic markers, (ii) high degree of infiltration and metastasis, and (iii)

© Claudio Ricci, Carlos Mota, Stefania Moscato, Delfo D'Alessandro, Stefano Ugel, Silvia Sartoris, Vincenzo Bronte, Ugo Boggi, Daniela Campani, Niccola Funel, Lorenzo Moroni, and Serena Danti
*Correspondence to: Lorenzo Moroni; Email: l.moroni@utwente.nl; Serena Danti; Email: s.danti@med.unipi.it
Submitted: 01/11/2014; Revised: 07/03/2014; Accepted: 08/10/2014
http://dx.doi.org/10.4161/21592527.2014.955386
This is an Open Access article distributed under the terms of the Creative Commons Attribution-Non-Commercial License (http://creativecommons.org/licenses/by-nc/3.0/), which permits unrestricted non-commercial use, distribution, and reproduction in any medium, provided the original work is properly cited. The moral rights of the named author(s) have been asserted.

strong resistance to conventional chemotherapy. Early detection of this disease thus seems to be the only means that would substantially impact patients' long-term survival. However, it has soon become evident that the accomplishment of this goal requires an in-depth understanding of PDAC biology, which is still a challenging subject of investigation.

The tumor is known to arise from the pancreatic duct system and to show epithelial features, but the precise origin of PDAC cells is still debated. Current data from genetically engineered mouse models indicate that PDAC is likely to develop from a metaplastic acinar-ductal cell.[3] Progression from a non-tumor tissue to infiltrating PDAC can start from different precursors, namely, pancreatic intraepithelial neoplasia (PanIN), intraductal papillary-mucinous neoplasm and cystic mucinous neoplasm.[4] The best characterized PDAC derives from PanIN passing through several stages up to the development of an in situ tumor.[5] Moreover, PDAC is able to attack the lymphatic system and distant organs very early and quickly, thus becoming highly metastatic even at the early stages.

In recent years, advances in cancer biology have highlighted that tumor microenvironment (TME) plays a pivotal role on cancer cell aggressiveness.[6] Tumors can recruit TME-supporting cells by modifying the normal tissue environment, e.g., cancer-associated fibroblasts, which are involved in carcinogenesis stimulation,[7,8] and tumor-associated macrophages, which become altered during cancer development.[9] Therefore, TME must be considered a dynamic entity remodeling with the tumor itself.

The TME of PDAC is particularly rich in stroma and very heterogeneous, as it comprises cellular and extracellular matrix (ECM) components.[10] Several cell types concur to generate the PDAC microenvironment, including fibroblasts, as well as pancreatic stellate, immune system, endothelial, cancer stem and PDAC cells.[11] To some extent, the failure of early PDAC diagnosis and the inefficiency of chemotherapy might be related to the convolution of its TME.[10] For complex tissue systems, like tumors, the traditional bi-dimensional (2D) in vitro models have revealed to be largely insufficient for drug screening and animal models have shown poor predictability.[12] Owing to the emerging importance of TME in the comprehension of carcinogenesis mechanisms, new biomimetic systems, such as 3-dimensional (3D) in vitro models, are currently the object of study.[13] It is a fact that an evolution from 2D to 3D models has occurred in the last decades.[13] In the simplest 3D models, cancer cells are usually agglomerated to form spheroids or embedded within biomaterial gels (e.g., Matrigel®, collagen).[13] Only very recently has the tissue engineering approach focused on cancer modeling, showing the intriguing possibility of generating complex 3D models in vitro.[14,15] Indeed, some TME characteristics can be recreated in advanced scaffold/cell systems.[16,17] Moreover, physical-chemical and mechanical phenomena regulating TME (e.g., cell-cell forces, matrix stiffness), transport phenomena (e.g., mass and energy transfer, fluid dynamics), and cellular kinetics (e.g., metabolism, signaling, proliferation) can be studied at the early stages, leading to new insights into the tumor-regulating key factors.[18,19]

In this study, we analyzed the interactions of primary PDAC cells with 3 different polymeric scaffolds. The use of primary cells, instead of immortalized cell lines, is of utmost importance to create biomimetic tumor models in which cells and TME do not show ab initio altered machinery.[20] We selected 3 types of scaffolds based on biocompatible polymeric formulations, such as poly(vinyl alcohol)/gelatin (PVA/G) mixture and poly(ethylene oxide terephthalate)/poly(butylene terephthalate) (PEOT/PBT) copolymer, manufactured with diverse architectures, such as sponge-like structures and nanofiber meshes. These polymers have been largely studied in tissue engineering applications and have shown optimal biocompatibility.[21,22] Since scaffold architecture and topography can play a key role in cell morphology and differentiation, we chose these types of polymeric scaffolds to assess a putatively different spatial arrangement of PDAC cells in sponge-like pores versus nanofiber mesh interspaces. The analyses on PDAC cell/scaffold constructs were aimed at assaying cell viability and colonization, cell/material interactions, cell morphology and supracellular organization. Finally, we investigated the production of matrix metalloproteinases (MMPs) as key enzymes involved in pancreatic cancer progression.[23,24] Our study reports on the effects of different scaffold types on human primary PDAC cells, as a first step to develop tumor-biomimetic 3D in vitro models potentially usable for therapeutic screening.

Results and Discussion

This study was aimed at investigating the interactions between human primary PDAC cells and polymeric scaffolds with different design and composition to create biomimetic models of PDAC. At such an early stage of scientific knowledge, it was important to identify some promising scaffold candidates that may steer further studies able to assess the role played by each specific parameter systematically. This goal was pursued through the accomplishment of 3 main objectives: (i) isolation of a primary PDAC cell line, (ii) fabrication of scaffolds with different internal architectures, and (iii) investigation of cell morphology and MMP-2 and MMP-9 expression after their culture within the selected scaffolds.

To develop functional tissue units ex vivo, tissue engineering has recently used strategies able to provide cells with the biomimetic cues of their original microenvironment, thus considering the cells as interactive entities highly integrated with their native niches.[25] In scientific practice, it has also become evident that primary cells retain their origin-related information necessary for biomimetic tissue development ex vivo. Indeed, immortalized cell lines frequently show altered replicative potential and they synthetize proteins at different levels and times if compared to those of primary cells.[20] To develop a tumor-biomimetic model, such considerations should also apply to cancer cells. As an example, we have reported that 3 commercial PDAC cell lines, all positive to Kirsten rat sarcoma viral oncogene homolog (K-ras) mutation, showed different responses to Ukrain (a semi-synthetic drug used to treat cancer) in terms of MMP-2 and MMP-9 production.[26] Cell lines are most easily accessible to researchers, but

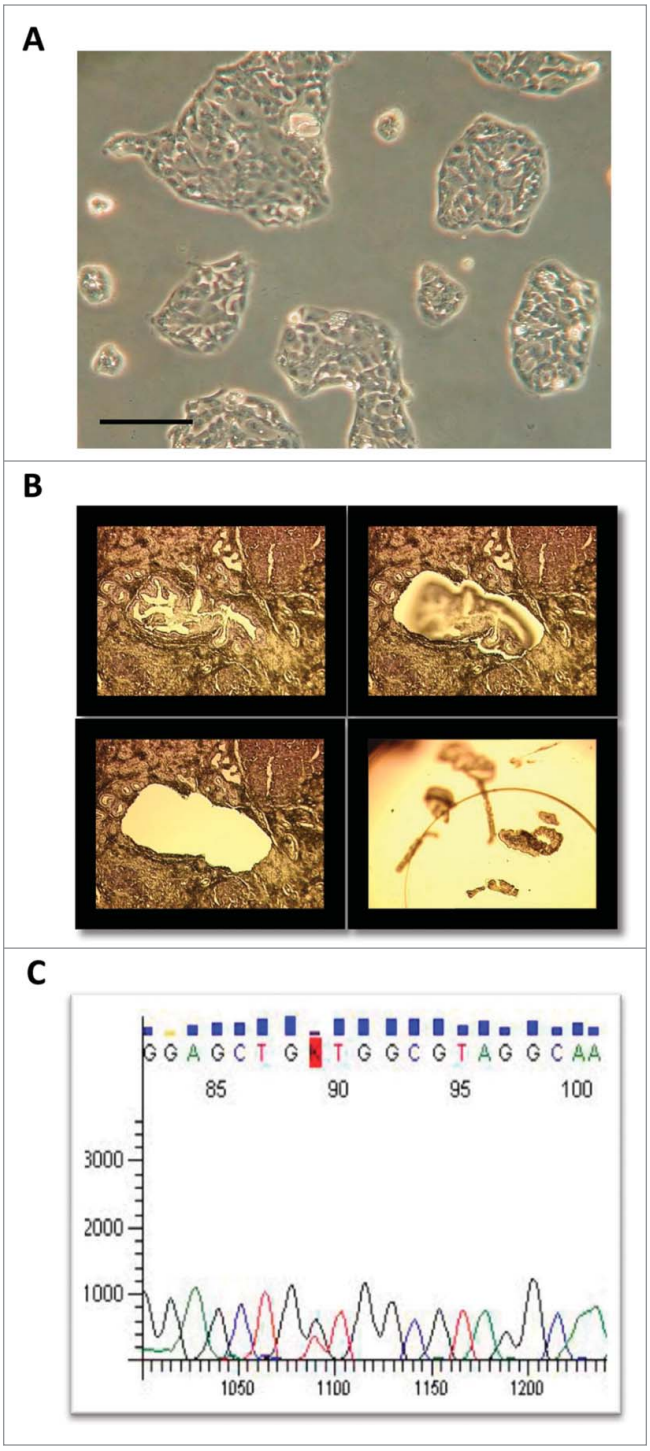

Figure 1. Isolation and characterization of the primary PDAC cell line NFCR01. (**A**) Micrograph of a pure population of epithelial PDAC cells, as obtained via contrast phase light microscopy (Original magnification 20×, scale bar = 50 μm). (**B**) Micrographs of laser microdissected epithelial cells from a PDAC fresh tissue to perform DNA extraction (Original magnification 10×). (**C**) K-ras gene mutation analysis of isolated cells showing G216T mutation in codon 12 of exon 2.

the use of primary cells isolated from tumor biopsies and characterized for their mutations, would provide a more representative TME and would therefore result in a model of increased reliability. The first objective of our study was to isolate and characterize primary human epithelial cells from PDAC explants (**Fig. 1A**). In order to demonstrate that the isolated cells retained genetic correspondence with the original tumor, we compared the purified cellular population in culture with the tumor cells obtained via laser microdissection (**Fig. 1B**). Mutations of K-ras have been found in almost 90% of PDACs.[27] In this view, the mutational status of K-ras gene can be considered as a fingerprint marker to assess the pancreatic tumor origin of isolated cell lines. All the commercial cell lines of pancreatic cancer show alteration in one out of 3 codons often mutated in PDAC tissues. In our study, the K-ras profile of the isolated cells showed a point gene mutation, namely G216T codon 12 of exon 2 (**Fig. 1C**). This mutation resulted to be identical to the one found in the cells microdissected from the tumor tissue, thus confirming that our cell line actually maintained the original hallmark of PDAC.

The second objective was to interface the primary cells with different types of scaffolds to assess their preferential affinity toward a specific architecture. A number of polymers and fabrication techniques have been used to produce 3D porous scaffolds for tissue engineering.[28] Conventional fabrication processes include salt leaching, gas forming, phase separation and freeze-drying to produce sponge-like matrices, or dry-, wet-, melt- and electro-spinning techniques to produce fiber meshes. Both spongy and fibrous scaffolds have been reported to support cell growth and differentiation.[29,30] However, the pore features of the scaffolds have shown to affect proliferation, spatial organization, differentiation and ECM production by cells, depending on the cell type.[28,29] Moreover, the cell function is directly influenced by their interaction with the surrounding environment, whether scaffold or native ECM. In line with these observations, it is important to select scaffolds with a cell type-appropriate architecture. We selected 3 different scaffold types that were produced via conventional scaffolding techniques. These methods enable high surface to volume ratio,[31] a parameter hypothesized to favor epithelial-like cell colonization. We used PVA/G sponge-like scaffolds produced via emulsion and freeze-drying, PEOT/PBT sponge-like scaffolds produced via compression molding and salt leaching, and PEOT/PBT fiber mesh scaffolds produced via electrospinning. The architectural features of the polymeric matrices were analyzed via scanning electron microscopy (SEM) (**Fig. 2**). PVA/G scaffolds appeared in the form of soft and hydrophilic sponges. They showed highly interconnected round-shaped pores with diameters ranging in 50-300 μm (**Fig. 2A1**). The pore walls were about 5–10 μm thick and had surfaces of diverse roughness (**Fig. 2A2**). PEOT/PBT sponge-like scaffolds resulted to be rigid. They displayed sufficiently interconnected cuboidal pores with diameters ranging in 300-500 μm (**Fig. 2B1**) that were surrounded by thick intraporal walls of about 80-200 μm and had smooth surfaces (**Fig. 2B2**). Finally, PEOT/PBT fibrous scaffolds appeared like a soft fabric of random fibers (**Fig. 2C1**), which showed a smooth

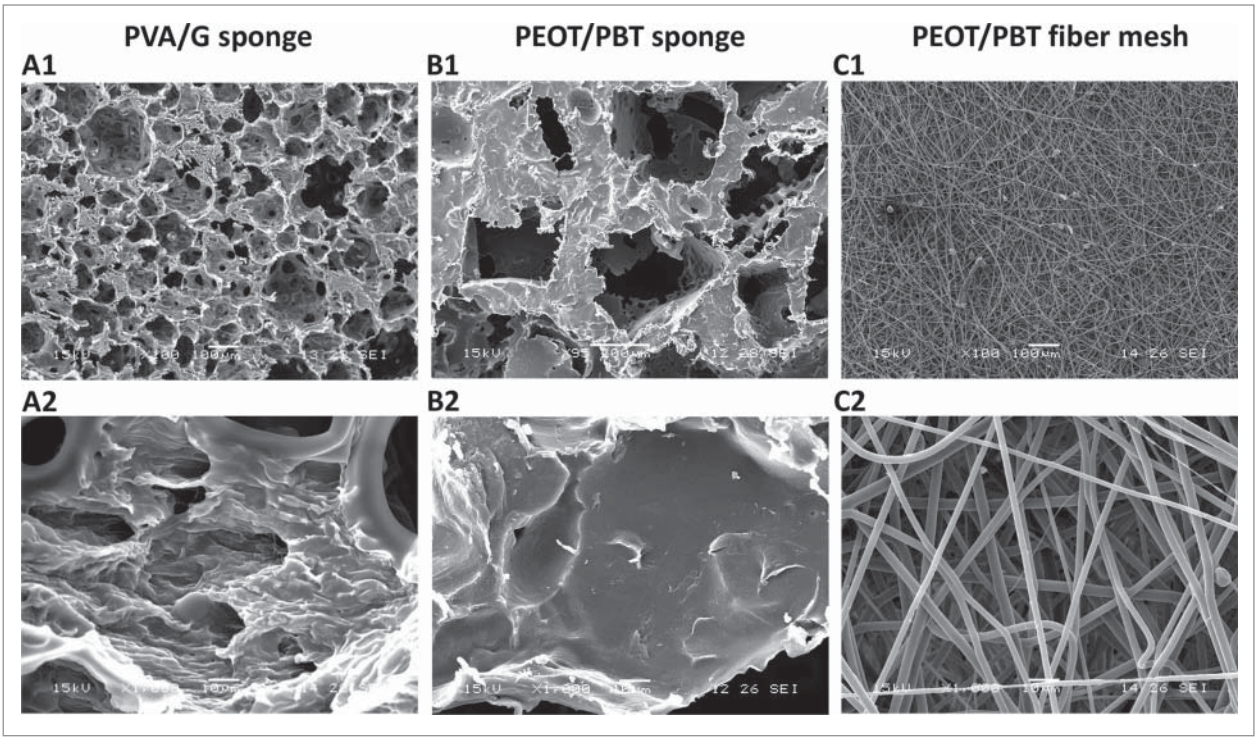

Figure 2. SEM micrographs of the produced scaffolds: (**A**) PVA/G sponge, (**B**) PEOT/PBT sponge, and (**C**) PEOT/PBT fiber mesh. Zoomed-out micrographs highlight pore size and topography (**A1–C1**), while zoomed-in micrographs image pore surfaces (**A2–C2**).

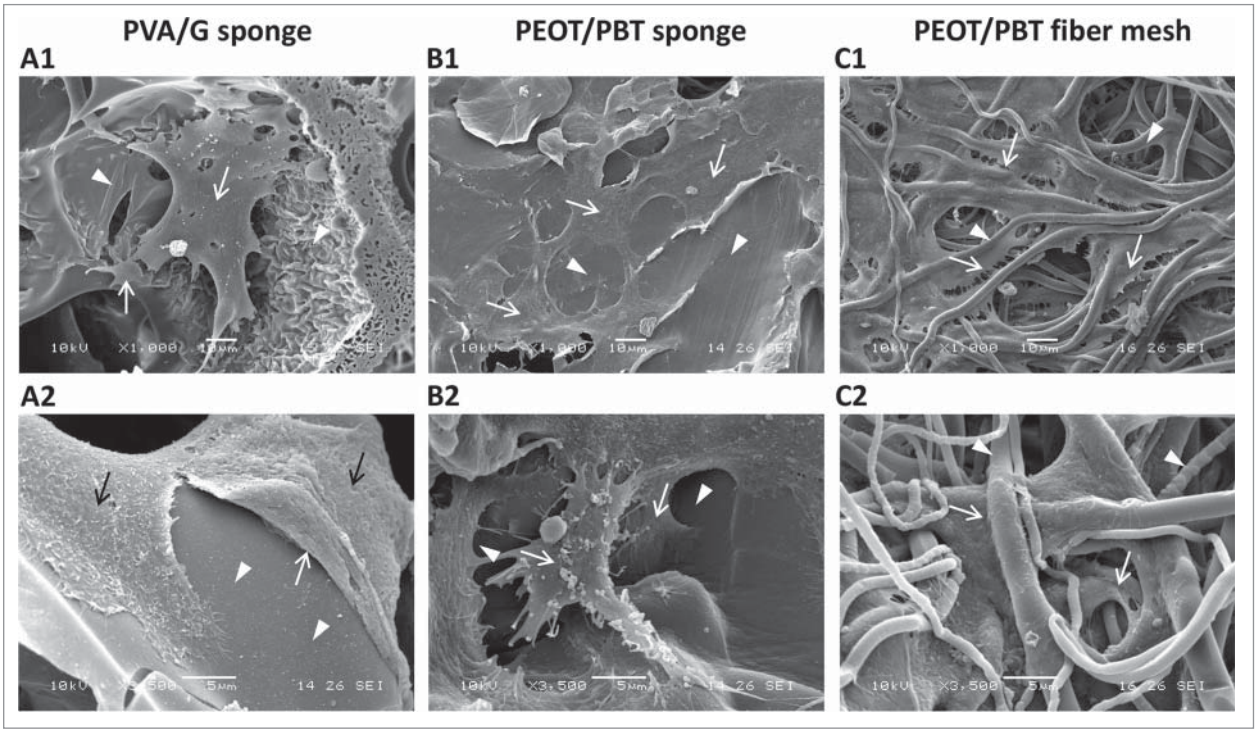

Figure 3. SEM micrographs of PDAC cell/scaffold constructs: (**A**) PVA/G sponge, (**B**) PEOT/PBT sponge, and (**C**) PEOT/PBT fiber mesh. Zoomed-out micrographs highlight interactions between cells and poral structures (**A1–C1**), while zoomed-in micrographs image single cells (**A2–C2**). Arrows indicate cells; arrowheads indicate scaffold surfaces.

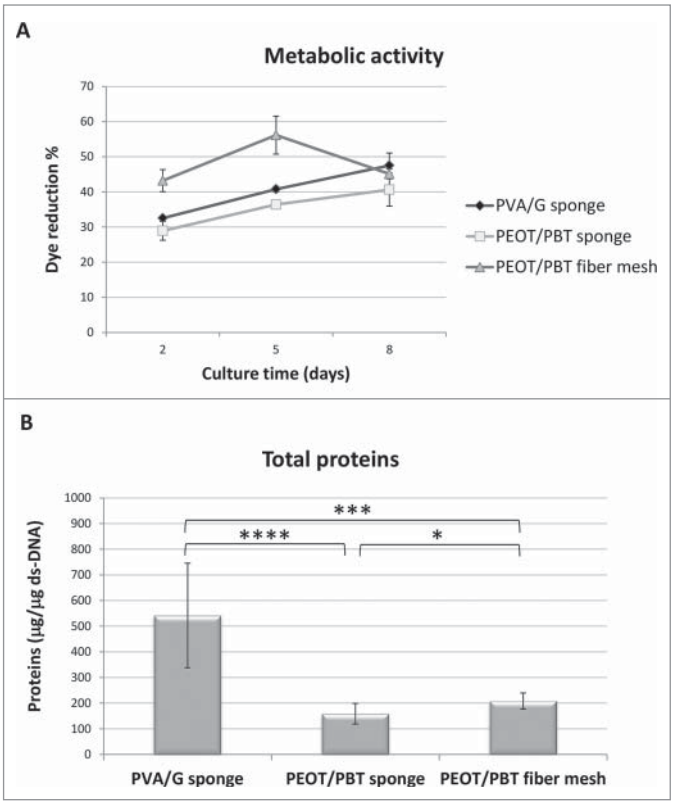

Figure 4. (**A**) Bar graph showing alamarBlue reduction percentage in PDAC cell/scaffold constructs along the culture time: PVA/G sponge, PEOT/PBT sponge, and PEOT/PBT fiber mesh. Data are reported as mean ± SD. Statistical analysis was performed at the endpoint ($P > 0.05$). (**B**) Bar graph showing total protein contents in PDAC cell/scaffold constructs at the culture endpoint. Data are reported as mean ± SD; asterisks indicate the following p values: * = 0.01; *** = 0.0001 and **** = 0.00005.

surface and homogenous diameters of about 1 μm (**Fig. 2C2**). Mesh thickness after collection was 220 ± 56 μm.

The third objective concerned the evaluation of cell/scaffold interactions. In the literature, only a few studies availing themselves of 3D models have been reported on pancreatic cancer. Simple 3D models are based on cellular spheroids obtained from PDAC cell lines. In these reports, tumor-derived cells have been embedded in methylcellulose or gelatin-fibronectin gels.[32,33] In a tissue engineering study, an electrospun scaffold of poly(glycolide-co-trimethylene carbonate)/G was used with pancreatic cancer stem cells.[34] Finally, a fibrous scaffold based on polyglyconate/G produced via electrospinning was tested with cancer stem cells as a model for pancreatic metastasis.[35] To our knowledge, no extensive investigation using spongy scaffolds in pancreas cancer modeling has been performed so far; instead, only electrospun microfiber meshes have been used in the few studies present in literature.[33-35] For this preliminary scaffold selection, 2 diverse polymeric sponges and an electrospun mesh were chosen, the latter being used to align our study with the current scientific background. Such scaffold types, cultured with normal (i.e., non-cancerous) cells, including fibroblasts and mesenchymal stem cells, resulted highly cytocompatible.[36-38] In this study, we investigated the interactions between these scaffold and primary PDAC cells, in terms of cell morphology and scaffold colonization. SEM analysis of cell/scaffold constructs, performed both on the top surface and in cross sections, revealed that pancreatic cells adhered on the inner surfaces of all the scaffold types we used. In the PVA/G sponges, the inner pores were well-colonized and the cells were extended across the pore walls (**Fig. 3A1**) or layered on their surfaces (**Fig. 3A1**). Similarly, in the PEOT/PBT sponges, the cells were well-stretched out on the biomaterial surfaces covering large scaffold areas (**Fig. 3B1**). Moreover, 3D cell placement with evidence of ECM molecule extrusion could be documented (**Fig. 3B2**). Differently, in the PEOT/PBT fibrous mesh, many cell protrusions were in contact with the scaffold fibers (**Fig. 3C1**) which, in some cases, were completely covered by cells (**Fig. 3C2**). Cell viability during culture was assessed using a metabolic test based on the alamarBlue® dye reduction percentage, which showed convergence of all the scaffolds at the endpoint, being 47.5 ± 3.5 %, 40.6 ± 4.7 % and 45 ± 1.4 % for PVA/G sponge, PEOT/PBT sponge and PEOT/PBT fiber mesh, respectively, with no statistically significant differences ($P > 0.05$) (**Fig. 4A**). The morphological and viability outcomes were confirmed by histologic analysis. Hematoxylin and eosin staining highlighted well-preserved cells with intact nuclei and cytoplasm (**Fig. 5A–C**). In both the spongy scaffold types, organized cell clusters showing a duct-like morphostructure could be imaged and appeared to be very similar to those of the tumor tissue (**Fig. 5A, B, and D**). Differently, these cellular structures could not be found on PEOT/PBT fiber meshes (**Fig. 5C1-3**). Of the 3 cell/scaffold constructs, the highest number of cell clusters with ductal formation was detected in the PVA/G scaffolds (**Fig. 5A1-3**). In our findings, PDAC cells are more likely to form tumor-biomimetic 3D aggregates inside sponge-like pores, than within nanofiber interspaces. Furthermore, the enhanced capability of organized cluster formation in PVA/G sponges can depend upon several factors, including chemical composition, pore size and shape, roughness, as well as mechanical features of the scaffold that deserve to be examined in future studies. It was also evident that the different architecture of PEOT/PBT scaffolds affected PDAC cell morphology.

Finally, we evaluated the MMP-2 and MMP-9 expression in the cell/scaffold constructs via IHC and Western Blot. MMPs are a family of proteases actively involved in ECM protein degradation. These proteases are synthesized by cells as latent proenzymes, which undergo activation by proteolytic cleavage of the full length proteins. Owing to their capability of TME remodeling via ECM disassembly, angiogenesis and inflammatory cell recruitment, MMPs have been directly correlated with

Table 1. IHC analysis of MMP antigen intensity

	PVA/G sponge	PEOT/PBT sponge	PEOT/PBT fiber mesh	Tumor
MMP-2	+/–	++	+/–	+++
MMP-9	+++	++++	++++	++++

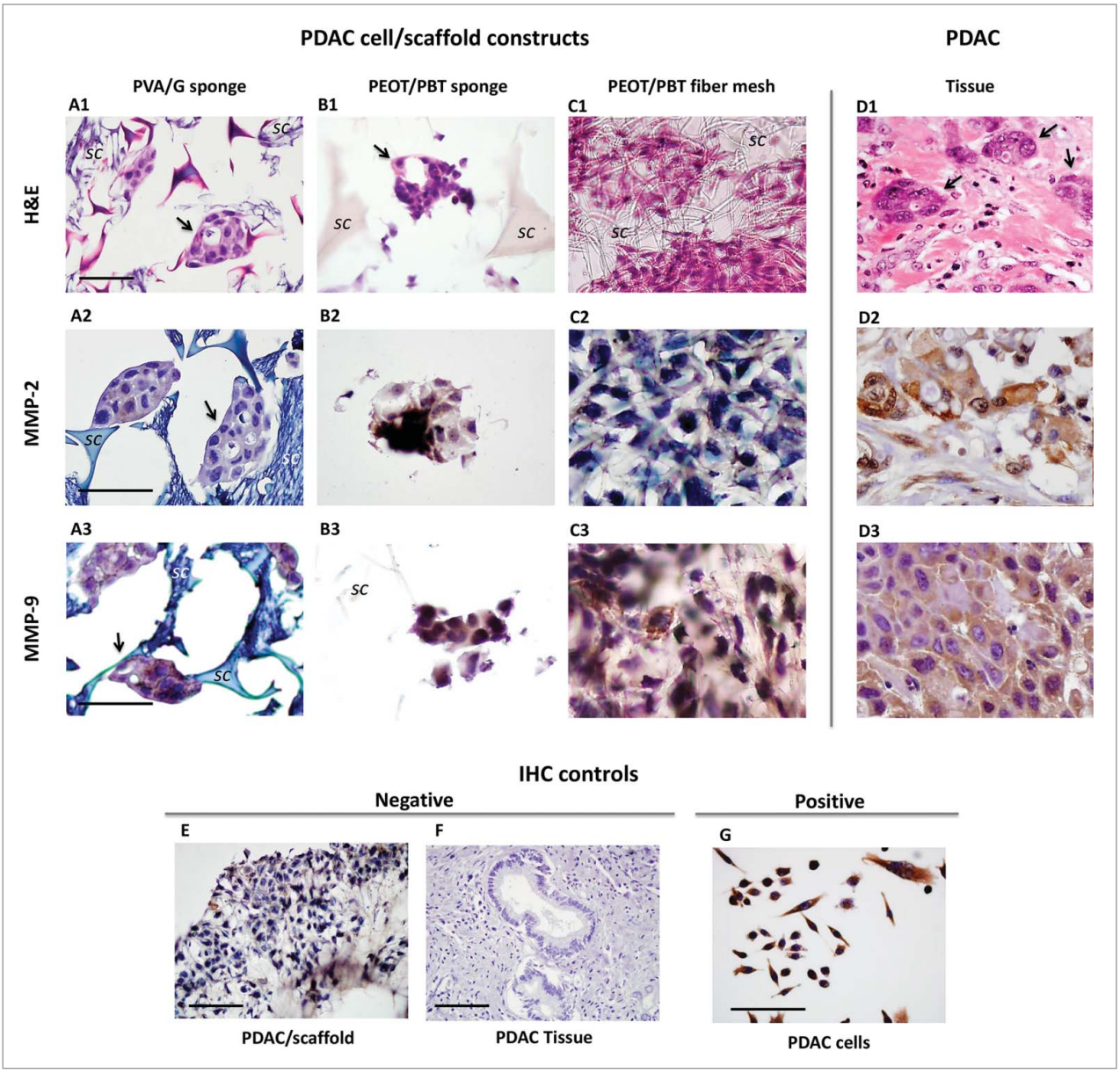

Figure 5. Light micrographs of histologic sections of PDAC cell/scaffold constructs (**A–C**) and tumor tissue (**D**): (**A**) PVA/G sponge, (**B**) PEOT/PBT sponge, and (**C**) PEOT/PBT fiber mesh. (**A1–D1**) Hematoxylin and eosin (H&E) staining, showing cell morphology (original magnification 20×), IHC of (**A2-D2**) MMP-2 and (**A3–D3**) MMP-9 (original magnifications 40×). Arrows indicate organized clusters of cell with duct formation; "sc" indicates the scaffold material. (**E–G**) Some controls of IHC reactions: (**E and F**) negative controls, i.e., omitting the primary antibody MMP-2, (**G**) positive control of MMP-2 performed on a PDAC cell line. Scale bar = 50 μm.

cancer development and invasion,[39] and indirectly with the metastatic processes as enablers of epithelial-mesenchymal transition. The role of some MMPs, such as MMP-2, MMP-7 and MMP-9, has been studied in PDAC.[26,40] MMP-2 and MMP-9 are frequently investigated in PDAC molecular pathways because of their connection with Smad4, which is a powerful tumor-suppression protein downregulated in PDAC progression.[27,40] It has been shown that K-ras gene mutation in concomitance with the loss of Smad4 mediates PDAC invasion through an increased MMP-9 expression.[27] Analysis of MMP antigen intensity as obtained via immunohistochemistry (IHC) is reported in **Table 1**. In our samples, IHC showed localized intracellular positivity of MMP-2 (**Fig. 5A2–D2**), which was most expressed in PEOT/PBT sponges (++) (**Fig. 5B2**), followed by PVA/G sponges (+/−) and PEOT/PBT nanofibers (+/−) (**Fig. 5A2 and C2**), if compared to the intensity of expression in the tumor tissue (+++) (**Fig. 5D2**). MMP-9 was intensely immunopositive in all 3 constructs (**Fig. 5A3-D3**). Antigen intensity in both PEOT/PBT scaffolds was ubiquitous and comparable to that of the tumor tissue (++++)

(**Fig. 5B3-D3**), while it appeared slightly reduced (+++) in PVA/G scaffolds. Here, some cell clusters appeared to be immunonegative (**Fig. 5A3**). These aspects could rely on different adaptations of the PDAC cells to the polymeric substrates. Bicinchoninic acid (BCA) assay performed on cell lysates and normalized by double-stranded (ds)-DNA content detected a diverse cellular synthesis of proteins in the 3 cell/scaffold constructs (**Fig. 4B**). The highest protein quantity produced per cell was found in the PVA/G sponges (541.73 ± 203.69 μg/μg ds-DNA, $p = 0.00005$ and $p = 0.0001$ vs. PEOT/PBT sponges and PEOT/PBT fiber meshes, respectively). A less powerful statistical difference ($p = 0.01$) was also highlighted between the 2 types of PEOT/PBT scaffolds, specifically, the total protein amount per cell resulted superior in the fiber meshes (208.64 ± 30.94 vs. 158.69 ± 40.24 μg/μg ds-DNA). These data indicate that a single PDAC cell was averagely able to synthesize more proteins in the PVA/G scaffolds than in both PEOT/PBT scaffolds. Taken together, the findings about protein production per cell and the metabolic activity of constructs suggest that PVA/G sponges may be selective scaffolds for PDAC cells, possibly representing a model of enhanced PDAC aggressiveness, with respect to both PEOT/PBT scaffolds in which cells displayed reduced synthesis activity.

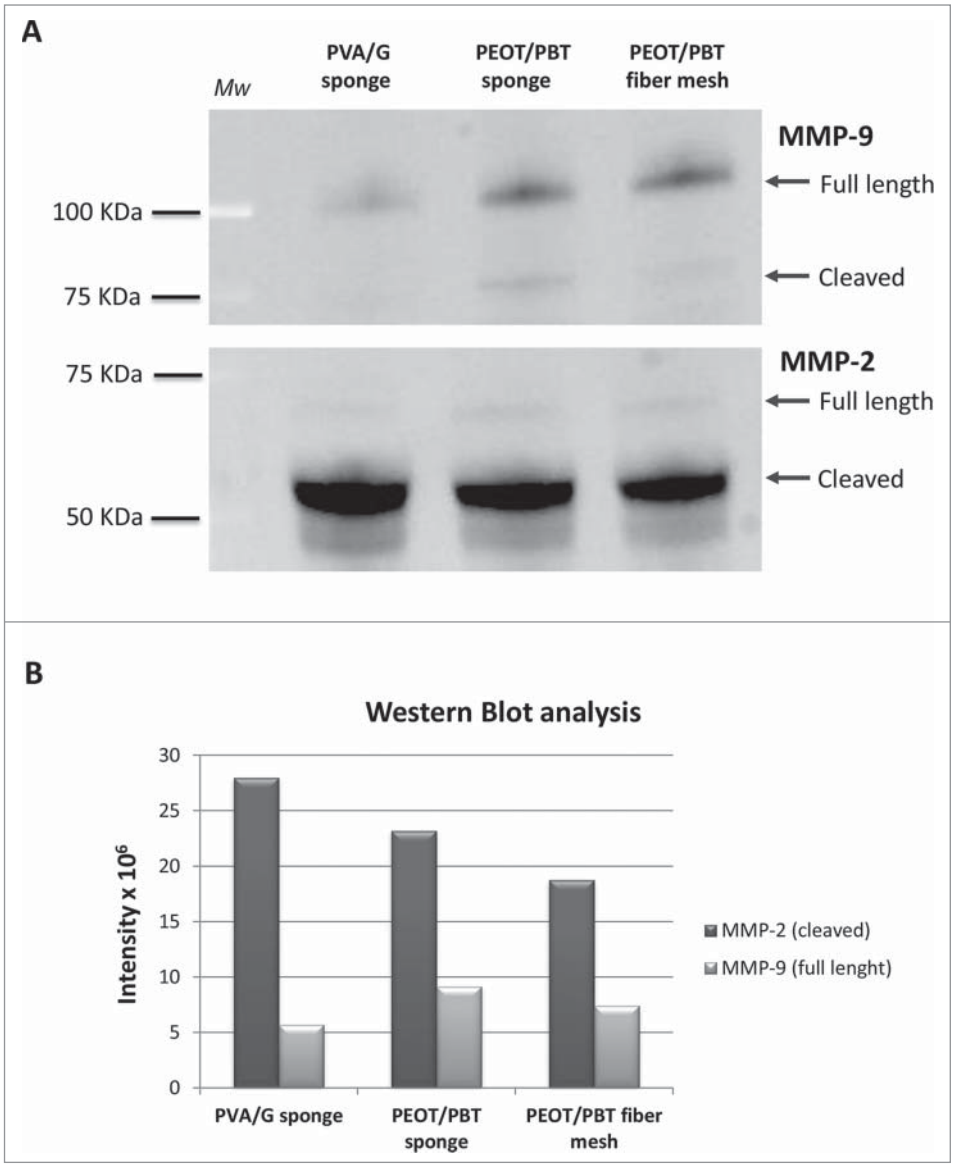

Figure 6. (**A**) Western blot results show the expression of MMP-2 and MMP-9 proteins, both in the active (cleaved) and inactive (full-length) forms in PVA/G sponge, PEOT/PBT sponge and PEOT/PBT fiber mesh. Molecular weight (Mw) scales are reported on the left. Arrows indicate the bands of interest. (**B**) Bar graph reporting the analysis of the band volume intensity for Western blot data (intensity × 10^6) for the 3 cell/scaffold constructs.

Finally, Western Blot analysis showed that cells grown on the different scaffolds expressed high levels of cleaved MMP-2 (the active enzyme), while the full length MMP-2 (the proenzyme) was expressed at low levels (**Fig. 6A**). Western Blot analysis also revealed a low expression of full length MMP-9, while the active enzyme was generally faintly detectable but in the PEOT/PBT sponge (**Fig. 6A**). The volume intensity analysis of Western Blot data was performed for the cleaved MMP-2 and full-length MMP-9, as the other lanes were not sufficiently detected (**Fig. 6B**). These quantitative results confirmed that the cleaved MMP-2 was more intensely expressed than the full length MMP-9 in all the constructs. The cleaved MMP-2 to full-length MMP-9 ratio reached 4.90 in the PVA/G constructs, while it was 2.53 in both construct types based on PEOT/PBT (both sponge and fiber mesh).

All in all, the obtained results indicated that the cleaved MMP-2 was the most abundant enzyme in our samples. However, from a comparative standpoint, our outcomes highlighted that both PEOT/PBT scaffold types stimulated the PDAC cells to produce MMP-9, although this was mainly detectable as a proenzyme, while PVA/G sponges best enhanced the expression of cleaved MMP-2. In addition, only the PEOT/PBT sponge was able to foster the cleaved MMP-9, suggesting that scaffold architecture may affect the function of primary PDAC cells. These slight variations of MMP levels still need to be clearly elucidated and further confirmed using primary PDAC cells from different patients. However, a differential stimulation of MMPs by diverse scaffolds could be

exploited to model a specific pathological status of clinical interest.

Among the investigated scaffolds, PVA/G sponges greatly favored primary PDAC cell organization in 3D clusters with duct-like morphostructure, enhanced the proteic synthesis of cells and in particular the production of active MMP-2. Therefore, it seemed to be a suitable scaffold for developing a biomimetic model of locally advanced PDAC. Moreover, PVA/G sponges could be processed with routine protocols used in the hospitals, appearing to be user-friendly models for cancer pathologists. On the other hand, PEOT/PBT sponges allowed for organized cell clustering with a large production of active MMP-2 and a reduced but significant production of active MMP-9. Finally, in the timeframe of our experiments, PEOT/PBT nanofiber meshes did not enable the formation of tumor-like aggregates by PDAC cells that synthetized active MMP-2 and inactive MMP-9. These scaffolds are most likely to mimic PDAC evolution at a different stage from that observed in the tumor biopsies. Owing to the late-stage diagnosis of this tumor, current knowledge on the early stages of PDAC evolution is still very limited. For these reasons, the putative relevance of PEOT/PBT electrospun scaffolds in PDAC modeling will deserve further discussion.

Materials and Methods

Ethical statement

The use of pancreas tumor tissue samples for research study was approved by the Ethics Committee of the Azienda Ospedaliero-Universitaria Pisana (AOUP), Pisa, Italy (Approval #3909-2013).

Isolation and culture of primary PDAC cells

PDAC pieces from surgery were washed extensively with phosphate-buffered saline (PBS) and cut into approximately 1 mm^3 fragments. These were plated onto 25 cm^2 tissue culture plastic flasks in RPMI-1640 medium (#F1255, Biochrom AG), supplemented with 10% fetal bovine serum (#10500, Gibco), 2 mM L-glutamine (#G7513, Sigma-Aldrich), 100 μg/ml streptomycin (#P0781, Sigma-Aldrich), 100 U/ml penicillin (#P0781, Sigma-Aldrich) and 1 mg/ml type XI Collagenase (c-9407, Sigma-Aldrich). The samples were cultured in a humidified incubator with 5% CO_2.[41] After 18 h, the cells sprout out from the explants were harvested and replated. The medium was replaced every 3 days, until cell colonies were identified. The primary PDAC cell line used in this study is NFCR01.

Laser microdissection, nucleic acid extraction and mutation analysis

Neoplastic cells were dissected from the tumor tissue using the Leica LMD6000 instrument (Leica, Wetzlar, Germany), as described in previous studies.[41,42] Laser-captured cells were harvested in lysis buffer for DNA extraction. The mutation analysis of the Kirsten rat sarcoma viral oncogene homolog (K-ras) was performed in both the microdissected tumor tissue and the tumor-derived primary cell culture to assess whether they matched the pancreatic tumor origin. Samples were resuspended in 20 μL of DNA extraction buffer, containing 0.005 M Tris-HCl, 0.001 M EDTA, 1% Tween-20 and 0.1 mg/ml proteinase K (pH 8.0), incubated overnight at 37°C, and proteinase-K inactivated at 95°C for 10 min. The gene mutational status of the K-ras coding exons (1-2) was determined by direct sequencing. Primers for polymer-chain reaction (PCR) were designed using the Primer3 program (available at http://bioinfo.ut.ee/primer3/). The annealing temperature used for PCR analysis was 57°C. The products were purified with the Montage PCR96 Cleanup Kit (#P36316, Millipore); thereafter, 6 μl of purified samples were sequenced using the BigDye Terminator v3.1 Cycle Sequencing Kit (Applied Biosystems). Sequencing was performed on an ABI PRISM 3100 Genetic Analyzer (Applied Biosystems), as reported in previous studies.[43]

Fabrication of PVA/G scaffolds

PVA/G scaffolds with 70/30 w/w composition ratio were obtained via emulsion and freeze-drying.[36] Briefly, an aqueous solution of PVA (#341584, Sigma-Aldrich) and G (#G6650, Sigma-Aldrich) was obtained at 50°C under stirring and further added with sodium lauryl sulfate to obtain a dense foam that was quenched in liquid nitrogen and lyophilized. Dried foams were stabilized by crosslinking with glutaraldehyde (GTA; #49630, Sigma-Aldrich) vapors for 72 h, flushed under the flow cabinet for 3 days, cut into cylinders (5 mm diameter, 3 mm thickness) and subsequently treated with 2 M glycine (#410225, Sigma-Aldrich) solution for 1 h to block GTA unreacted binding sites. The resulting sponge is a highly porous, biocompatible, hydrophilic and bio-stable material, suitable for tissue engineering applications.[36]

Fabrication of PEOT/PBT scaffolds

PEOT/PBT copolymers were obtained from PolyVation B.V., The Netherlands. Sponge-like PEOT/PBT (300PEOT55PBT45) scaffolds were prepared using a compression molding and particle-leaching method, as previously reported.[37] A copolymer/salt granule mixture was prepared with 400-600 μm granulometry and a final salt volume percentage of 75%. The mixture was heated to 180 °C for 3 min followed by compression molding for 1 min at 2.9 MPa inside a hot press (THB 008, Fontijne Holland BV, The Netherlands), thus resulting in 120 × 100 × 10 mm^3 blocks. The salt was leached out by washing in demineralized water for 48 h. Finally, the samples were dried under reduced pressure in a vacuum oven and cut into cylinders (5 mm diameter, 3 mm thickness) with a puncher.

An electrospinning apparatus was used to prepare PEOT/PBT copolymer fiber meshes. A 20% w/v solution of 300PEOT55PBT45 was prepared in a solvent mixture of $CHCl_3$ and HFIP (90/10% v/v), as previously reported.[30] The solution was introduced in a plastic syringe and placed on a syringe pump (KDS 100, KD Scientific) to control polymer dispensing through a spinneret. The following manufacturing parameters were chosen: constant feed rate of 5 ml/h, a voltage of 15 kV and a distance between the spinneret and the collector of 15 cm. The spinneret (21-gauge blunt tip) was positively charged and the

collector was grounded. A rotating drum collector with rotational velocity of 150 r.p.m. was used to produce and keep the mesh thickness constant. Manufacturing was performed under controlled environmental conditions (temperature of 25 ± 1°C and 30% humidity) and fiber collection time was 30 min.

After production, the PEOT/PBT scaffolds were treated with argon (Ar) plasma to improve cell adhesion by changing surface roughness.[44] The scaffolds were placed inside a radio-frequency glow-discharge chamber (Harrick Scientific Corp., NY, USA) and a pre-vacuum was applied. Thereafter, Ar gas was flushed for 30 min under controlled 0.1–0.2 mbar vacuum with high settings applied to the radio-frequency coil (740 V DC, 40 mA DC, 29.6 W).

Culture of PDAC/scaffold constructs

The scaffolds (n = 5) were sterilized by overnight soaking in absolute ethanol, washed 3 times with sterile 2× Pen-Strep (#P0781, Sigma-Aldrich)/Diflucan (Pfizer) saline and rinsed with PBS prior to cell seeding. PDAC cells were seeded on the scaffolds at a density of 1×10^4 cells/mm^3 of scaffold volume in 30 μl of culture medium, then the samples were placed for 1 h in the incubator for cell adhesion. The specimens were fully covered with complete RMPI medium and cultured for 9 days providing media changes every 3 days.

Scanning electron microscopy (SEM)

SEM was used to analyze the architectural features of the plain scaffolds and cell adhesion to the scaffold surfaces. Cellularized samples underwent preliminary fixation (4% neutral buffered formalin in PBS, overnight at 4°C), dehydration in a graded series of ethanol aqueous solutions up to anhydrous ethanol, drying by the critical point method (Balzers CPD030, Oerlikon Balzers, Balzers, Liechtenstein), and cross-sectioning. Samples were mounted on aluminum stumps, sputter-coated with gold (Edwards Sputter Coater S150B, Edwards, NY, USA) and examined with a scanning electron microscope (JEOL JSM-5600 LV, JEOL Ltd, Tokyo, Japan).

AlamarBlue® assay

The viability of cell/scaffold constructs was investigated using the alamarBlue® assay (#BUF012A, Serotec Ltd). This bioassay incorporates a REDOX indicator resulting in color change of the culture medium according to cell metabolism. Owing to its negligible toxicity, this assay can be performed multiple times on the same samples. Samples and controls (including scaffolds with no cells as blank controls), were incubated with the dye for 3 h according to the manufacturer's recommendations. Samples were assayed at different culture time points 2, 5 and 8 days to assess cell viability. After each assay, the supernatants were removed from the cultures and replaced with fresh culture medium. The samples were analyzed with a spectrophotometer (Victor3, PerkinElmer, Waltham, MA, USA) under a double wavelength reading, 570 nm and 600 nm. Finally, dye reduction percentage was calculated using dye molar extinction coefficients and appropriate absorbance equations as provided by the manufacturer.

Total proteins and ds-DNA

Total protein and ds-DNA assays were carried out in cascade on the same samples (n = 3) for value normalization. At the culture endpoint, the medium was removed from the constructs and double distilled (dd)-water was added (2 ml/sample). These samples were frozen at −80°C and stored. Plain PVA/G scaffold controls were performed to subtract putatively scaffold-released from cell-produced proteins. To enable both the proteins and the ds-DNA to enter the solution, cell lysates were obtained performing 3 freeze/thaw cycles of the samples. Each cycle consisted of 10 min thawing at 37°C in a sonicator bath (Bransonic 2510, Bransonic, Danbury, CT, USA), followed by 10 min quenching in liquid nitrogen. Ds-DNA content in cell lysates was measured using the PicoGreen kit (Quant-iT™, #P7589, Molecular Probes, Invitrogen). The PicoGreen dye binds to ds-DNA and the resulting fluorescence intensity is directly proportional to ds-DNA concentration in solution. Standard solutions of DNA in dd-water at concentrations ranging from 0–6 μg/ml were prepared and 50 μl of standard or sample was loaded for quantification in a 96-well black microplate. Working buffer and PicoGreen dye solution were prepared according to the manufacturer's instructions and added at 100 and 150 μl per well, respectively. After a 10 min incubation at room temperature in the dark, the fluorescence intensity was measured on a plate reader (Victor3; PerkinElmer, Waltham, MA) using an excitation wavelength of 485 nm and an emission wavelength of 535 nm.

The total protein concentration was determined by the BCA method (#23225, Pierce Biotechnology, Rockford, IL) following the microplate procedure. Cell lysates and the working reagent were loaded inside a 96-well microplate at 25 and 200 μl per well, respectively. The microplate was incubated at 37°C for 30 min. Samples were cooled down to room temperature and absorbance was read at 562 nm on a plate reader (BioRad Laboratories, Hercules, CA). Protein concentration of cellular specimens was then obtained by reference to bovine serum albumin (BSA) standards. Finally, total protein content was normalized by DNA content as determined by the PicoGreen assay.

Histological analysis

For tumor characterization, 5 μm-thick frozen tissue sections were thawed and fixed in 75% ethanol. The cell/scaffold constructs were treated for paraffin embedding. They were fixed in 4% neutral buffered formalin overnight at 4°C and washed in 1× PBS. Constructs of PDAC cells and PVA/G sponges could be processed using routine protocols for surgical pathology specimens. Other scaffolds required modified procedures for histologic processing, as reported hereafter. Constructs based on PEOT/PBT sponges were dehydrated with a graded series of ethanol aqueous solutions for extended times (4 h each step), up to absolute ethanol (30 h). The specimens were clarified in xylene at 58°C for 2 h. Constructs based on PEOT/PBT fiber meshes were dehydrated with a graded series of ethanol aqueous solutions up to absolute ethanol (6 h) and clarified in xylene at 40°C for 90 min. All samples were then soaked in liquid paraffin at 60°C for 2 h and paraffin-embedded. A standard microtome allowed 8 μm-thick sections to be obtained that were mounted on slides

and dried at 37°C. Samples were then rehydrated using xylene and ethanol solutions. Finally, sections of tumor tissue and cell/scaffold constructs were stained with hematoxylin and eosin for morphologic analysis.

Immunohistochemistry (IHC)

The protein expression of both MMP-2 and MMP-9 was examined by IHC in the tumor models and in the tumor tissue, the latter as a positive control. Formalin-fixed sections were hydrated. Antigen retrieval was performed through soaking 3 times for 3 minutes in 10 mM citrate buffer pH 6 at 96°C. The sections were treated for endogenous peroxidase quenching, by incubating the specimens in a 3% H_2O_2 solution at room temperature in the dark for 15 min. Samples were incubated with monoclonal mouse anti-human MMP-2 or MMP-9 antibodies (#4022 and #3852, respectively, CST Cell Signaling, Inc.) at 1:100 dilution for 1 h and stained with avidin-biotin-peroxidase complex (Revealing Kit #951D-22 and DAB substrate Kit #957D-22, Cell Marque). The sections were counterstained with hematoxilyn. Negative controls for both the cell/scaffold constructs and the tumor were obtained by replacement of the primary antibody with buffer. Antigen positivity was scored according to the following criteria: − = negative; + = weakly positive; ++ = positive; +++ = strongly positive; ++++ = very strongly positive.

Western Blot

The MMP-2 and MMP-9 expression was evaluated by Western Blot analysis at the end point. Briefly, cell/scaffold constructs were resuspended in lysis buffer (50 mM Tris-HCl, pH 7.4, 150 mM NaCl, 2 mM EDTA, 1% NP-40) added with antiproteases 1× (#S8830, Sigma-Aldrich). The samples were maintained in ice for 1 h and vortexed every 10 min for mechanical disruption. Protein concentration was determined using the BCA microplate method (#23225, Thermo Fisher). Equal quantities of proteins (20 μg/sample) were separated on a 4–15% polyacrylamide gel (#4561083, BioRad) under reducing conditions, and then transferred to a nitrocellulose membrane (#1704158, Trans Turbo Blot system, BioRad). The membranes were blocked with 4% dry fat milk in 0.1% TBS Tween (T-TBS) and incubated with either rabbit polyclonal anti MMP-2 or anti MMP-9 (#4022 and #3852, respectively, CST Cell Signaling, Inc.) diluted in 5% bovine serum albumin (BSA) in T-TBS, at concentrations of 1:1000 and 1:500, respectively, at 4°C overnight. An anti-rabbit horseradish peroxidase (HRP)-conjugated antibody (#074-1506, KPL), diluted 1:2000 in 5% BSA in T-TBS, at room temperature for 1 h was used as secondary antibody and immunocomplexes were detected by chemiluminescence (#170-5061, ECL clarity, BioRad) using Chemi-Doc XRS+ (BioRad). The data were analyzed using Image Lab software (BioRad).

Statistical analysis

Statistical significance in quantitative analyses was evaluated using the 2-tailed t test for either paired (alamarBlue assay) or unpaired (Total Protein assay) data, followed by Bonferroni's correction. The data underwent both descriptive, i.e., mean ± standard deviation (SD), and inferential statistics (p-values).

Conclusion

In this study, we investigated the interactions of primary PDAC cells with 3 different polymeric scaffolds, based on biocompatible polymers (PVA/G mixture and PEOT/PBT copolymer) and manufactured so as to have different inner architectures. Analyses showed that PDAC cells were viable inside the 3 scaffolds after a 9-day culture and that they synthesized tumor-specific MMPs, such as MMP-2 and MMP-9. Interestingly, independently of the polymer formulation, sponge-like pores (50–500 μm diameter) allowed cellular clustering similar to the native cancer morphostructure. However, the highest number of PDAC clusters with early ductal formations were observed in the PVA/G scaffolds. These findings demonstrate that pore size and topography, as well as polymer chemistry, can affect the spatial organization of PDAC cells ex vivo; furthermore, poral structures originated from nanofiber interspaces prevented clustered formations by PDAC cells. In our samples, the cleaved MMP-2 was the most abundantly produced enzyme. However, some slight differences could be highlighted. In PVA/G sponges the active MMP-2 enzyme resulted to be higher to the detriment of inactive MMP-9 than the ones detected in the other scaffolds. On the other hand, PEOT/PBT sponges stimulated some production of active MMP-9 together with active MMP-2. Instead, the cells inside PEOT/PBT nanofibers mainly synthesized inactive MMP-9 and slightly reduced MMP-2. This indicates that the PVA/G and PEOT/PBT spongy constructs could mimic pancreatic tumor models at locally advanced stages. In conclusion, PDAC cells showed diverse behavior when interacting with different scaffold types that can be exploited to model various phases of pancreatic tumor development and invasion. The availability of advanced 3D in vitro models of PDAC could be employed in the near future to screen drug susceptibility and MMP modulation, according to specific interactions with the pancreatic TME.

Disclosure of Potential Conflicts of Interest

No potential conflicts of interest were disclosed.

Acknowledgments

The Italian Association for Cancer Research (AIRC) is acknowledged for contributing to this study. The authors thank Dr. Randa Ishak (Dept. of Civil and Industrial Engineering, University of Pisa, Italy) for her SEM technical support.

Funding

This research was funded by the Italian Ministry of University and Research (MIUR) (PRIN #2009FZZ4XM), Istituto Toscano Tumori (ITT) (approval number 6204-2012).

References

1. Siegel R, Naishadham D, Jemal A. Cancer statistics, 2012. CA Cancer J Clin 2012; 62:10-29; PMID:22237781; http://dx.doi.org/10.3322/caac.20138
2. Vincent A, Herman J, Schulick R, Hruban RH, Goggins M. Pancreatic cancer. Lancet 2011; 378:607-20; PMID:21620466; http://dx.doi.org/10.1016/S0140-6736(10)62307-0
3. Esposito I, Konukiewitz B, Schlitter AM, Klöppel G. New insights into the origin of pancreatic cancer: role of atypical flat lesions in pancreatic carcinogenesis. Pathologe 2012; 33:189-93; PMID:23011021; http://dx.doi.org/10.1007/s00292-012-1673-x
4. Maitra A, Hruban RH. Pancreatic cancer. Annu Rev Pathol 2008; 3:157-88; PMID:18039136; http://dx.doi.org/10.1146/annurev.pathmechdis.3.121806.154305
5. Herreros-Villanueva M, Gironella M, Castells A, Bujanda L. Molecular markers in pancreatic cancer diagnosis. Clin Chim Acta 2013;418:22-9; PMID:23305796; http://dx.doi.org/10.1016/j.cca.2012.12.025
6. Quail DF, Joyce JA. Microenvironmental regulation of tumor progression and metastasis. Nat Med 2013; 19:1423-37; PMID:24202395; http://dx.doi.org/10.1038/nm.3394
7. Olumi, AF, Olumi AF, Grossfeld GD, Hayward SW, Carroll PR, Tlsty TD, Cunha GR. Carcinoma-associated fibroblasts direct tumor progression of initi-ated human prostatic epithelium. Cancer Res 1999; 59:5002-11; PMID:10519415
8. Dumont N, Dumont N, Liu B, Defilippis RA, Chang H, Rabban JT, Karnezis AN, Tjoe JA, Marx J, Parvin B, et al. Breast fibroblasts modulate early dissemination, tumorigenesis, and metastasis through. Neoplasia 2013; 15:249-62; PMID:23479504
9. Qian BZ, Pollard JW. Macrophage diversity enhances tumor progression and metastasis. Cell 2010; 141:39-51; PMID:20371344; http://dx.doi.org/10.1016/j.cell.2010.03.014
10. Feig C, Gopinathan A, Neesse A, Chan DS, Cook N, Tuveson DA. Pancreas Cancer Microenvironment Clin Cancer Res 2012; 18:4266-76.
11. Iovanna J, Mallmann MC, Gonçalves A, Turrini O, Dagorn JC. Current knowledge on pancreatic cancer. Front Oncol 2012; 31:2-6.
12. Voskoglou-Nomikos T, Pater JL, Seymour L. Clinical predictive value of the in vitro cell line, human xenograft, and mouse allograft preclinical cancer models. Clin Cancer Res 2003; 9:4227-39; PMID:14519650
13. Kim JB. Three-dimensional tissue culture models in cancer biology. Semin Cancer Biol 2005; 15:365-77; PMID:15975824; http://dx.doi.org/10.1016/j.semcancer.2005.05.002
14. Hutmacher DW, Horch RE, Loessner D, Rizzi S, Sieh S, Reichert JC, Clements JA, Beier JP, Arkudas A, Bleiziffer O, et al. Translating tissue engineering technology platforms into cancer research. J Cell Mol Med 2009; 13(8A):1417-27; PMID:19627398; http://dx.doi.org/10.1111/j.1582-4934.2009.00853.x
15. Ghajar CM, Bissell MJ. Tumor engineering: the other face of tissue engineering. Tissue Eng Part A 2010; 16:2153-6; PMID:20214448; http://dx.doi.org/10.1089/ten.tea.2010.0135
16. Burdett E, Kasper FK, Mikos AG, Ludwig JA. Engineering tumors: a tissue engineering perspective in cancer biology. Tissue Eng Part B Rev 2010;6:351-9; PMID:20092396; http://dx.doi.org/10.1089/ten.teb.2009.0676
17. Ricci C, Moroni L, Danti S. Cancer tissue engineering: new perspectives in understanding the biology of solid tumors. A critical review. OA Tissue Eng 2013; 1:4; http://dx.doi.org/10.13172/2052-9643-1-1-607
18. DelNero P, Song YH, Fischbach C. Microengineered tumor models: insights & opportunities from a physical sciences-oncology perspective. Biomed Microdevices 2013; 15:583-93; PMID:23559404; http://dx.doi.org/10.1007/s10544-013-9763-y
19. Hutmacher DW, Loessner D, Rizzi S, Kaplan DL, Mooney DJ, Clements JA. Can tissue engineering concepts advance tumor biology research? Trends Biotechnol 2010; 28(3):125-33; PMID:20056286; http://dx.doi.org/10.1016/j.tibtech.2009.12.001
20. Czekanska EM, Stoddart MJ, Ralphs JR, Richards RG, Hayes JS. A phenotypic comparison of osteoblast cell lines versus human primary osteoblasts for biomaterials testing. J Biomed Mater Res A 2013; 102:2636-43; PMID:23983015; http://dx.doi.org/10.1002/jbm.a.34937
21. DeMerlis CC, Schoneker DR. Review of the oral toxicity of polyvinyl alcohol (PVA). Food Chem Toxicol 2003; 41:319-26; PMID:12504164; http://dx.doi.org/10.1016/S0278-6915(02)00258-2
22. Bartha L, Hamann D, Pieper J, Péters F, Riesle J, Vajda A, Novak PK, Hangody LR, Vasarhelyi G, Bodó L, et al. A clinical feasibility study to evaluate the safety and efficacy of PEOT/PBT implants for human donor site filling during mosaicplasty. Eur J Orthop Surg Traumatol 2013; 23:81-91; PMID:23412412; http://dx.doi.org/10.1007/s00590-011-0907-6
23. Singh N, Das P, Datta Gupta S, Sahni P, Pandey RM, Gupta S, Chauhan SS, Saraya A. Prognostic significance of extracellular matrix degrading enzymes-cathepsin L and matrix metalloproteases-2 [MMP-2] in human pancreatic cancer. Cancer Invest 2013; 31:461-71.
24. Ellenrieder V, Alber B, Lacher U, Hendler SF, Menke A, Boeck W, Wagner M, Wilda M, Friess H, Büchler M, et al. Role of MT-MMPs and MMP-2 in pancreatic cancer progression. Int J Cancer 2000; 85:14-20; PMID:10585576; http://dx.doi.org/10.1002/(SICI)1097-0215(20000101)85:1<14::AID-IJC3>3.0.CO;2-O
25. Ingber DE, Mow VC, Butler D, Niklason L, Huard J, Mao J, Yannas I, Kaplan D, Vunjak-Novakovic G. Tissue engineering and developmental biology: going biomimetic. Tissue Eng 2006; 12:3265-83; PMID:17518669; http://dx.doi.org/10.1089/ten.2006.12.3265
26. Funel N, Costa F, Pettinari L, Taddeo A, Sala A, Chiriva-Internati M, Cobos E, Colombo G, Milzani A, Campani D, et al. Ukrain affects pancreas cancer cell phenotype in vitro by targeting MMP-9 and intra-/extracellular SPARC expression. Pancreatology 2010; 10:545-52; PMID:20975318; http://dx.doi.org/10.1159/000266127
27. Bera A, Zhao S, Cao L, Chiao PJ, Freeman JW. Oncogenic K-Ras and loss of Smad4 mediate invasion by activating an EGFR/NF-κB axis that induces expression of MMP9 and uPA in human pancreas progenitor cells. PLoS One 2013; 8:e82282; PMID:24340014; http://dx.doi.org/10.1371/journal.pone.0082282
28. Loh QL, Choong C. Three-dimensional scaffolds for tissue engineering applications: role of porosity and pore size. Tissue Eng Part B Rev 2013; 19:485-502; PMID:23672709; http://dx.doi.org/10.1089/ten.teb.2012.0437
29. Mallick KK, Cox SC. Biomaterial scaffolds for tissue engineering. Front Biosci (Elite Ed) 2013; 5:341-60; PMID:23276994
30. Ingavle GC, Leach JK. Advancements in electrospinning of polymeric nanofibrous scaffolds for tissue engineering. Tissue Eng Part B Rev 2014; 20(4):277-93.
31. Hutmacher DW. Scaffold design and fabrication technologies for engineering tissues–state of the art and future perspectives. J Biomater Sci Polym Ed 2001; 12:107-24; PMID:11334185; http://dx.doi.org/10.1163/156856201744489
32. Longati P, Jia X, Eimer J, Wagman A, Witt MR, Rehnmark S, Verbeke C, Toftgård R, Lohr M, Heuchel RL. 3D pancreatic carcinoma spheroids induce a matrix-rich, chemoresistant phenotype offering a better model for drug testing. BMC Cancer 2013; 13:95; PMID:23446043; http://dx.doi.org/10.1186/1471-2407-13-95
33. Hosoya H, Kadowaki K, Matsusaki M, Cabral H, Nishihara H, Ijichi H, Koike K, Kataoka K, Miyazono K, Akashi M, et al. Engineering fibrotic tissue in pancreatic cancer: a novel three-dimensional model to investigate nanoparticle delivery. Biochem Biophys Res Comm 2012; 419:32-7; PMID:22321398; http://dx.doi.org/10.1016/j.bbrc.2012.01.117
34. He Q, Wang X, Zhang X, Han H, Han B, Xu J, Tang K, Fu Z, Yin H. A Tissue engineered subcutaneous pancreatic cancer model for antitumor drug evaluation. Int J Nanomedicine 2013; 8:1167-76; PMID:23658483; http://dx.doi.org/10.2147/IJN.S42464
35. Wang X, Zhang X, Fu Z, Yin H. A bioengineered metastatic pancreatic tumor model for mechanistic investigation of chemotherapeutic drugs. J Biotechnol 2013; 166:166-73; PMID:23747489; http://dx.doi.org/10.1016/j.jbiotec.2013.05.008
36. Moscato S, Mattii L, D'Alessandro D, Cascone MG, Lazzeri L, Serino LP, Dolfi A, Bernardini N. Interaction of human gingival fibroblasts with PVA/gelatine sponges. Micron 2008; 39:569-79; PMID:17702585; http://dx.doi.org/10.1016/j.micron.2007.06.016
37. Du C, Klasens P, Haan RE, Bezemer J, Cui FZ, de Groot K, Layrolle P. Biomimetic calcium phosphate coatings on Polyactive 1000/70/30. J Biomed Mater Res 2002; 59:535-46; PMID:11774312; http://dx.doi.org/10.1002/jbm.1267
38. Moroni L, Licht R, de Boer J, de Wijn JR, van Blitterswijk CA. Fiber diameter and texture of electrospun PEOT/PBT scaffolds influence human mesenchymal stem cell proliferation and morphology, and the release of incorporated compounds. Biomaterials 2006; 27:4911-22; PMID:16762409; http://dx.doi.org/10.1016/j.biomaterials.2006.05.027
39. Coussens LM, Fingleton B, Matrisian LM. Matrix metalloproteinase inhibitors and cancer: trials and tribulations. Science 2002; 295:2387-92; PMID:11923519; http://dx.doi.org/10.1126/science.1067100
40. Wiercinska E, Naber HP, Pardali E, van der Pluijm G, van Dam H, ten Dijke P. The TGF-β/Smad pathway induces breast cancer cell invasion through the up-regulation of matrix metalloproteinase 2 and 9 in a spheroid invasion model system. Breast Cancer Res Treat 2011; 128:657-66; PMID:20821046; http://dx.doi.org/10.1007/s10549-010-1147-x
41. Funel N, Giovannetti E, Del Chiaro M, Mey V, Pollina LE, Nannizzi S, Boggi U, Ricciardi S, Del Tacca M, Bevilacqua G, et al. Laser microdissection and primary cell cultures improve pharmacogenetic analysis in pancreatic adenocarcinoma. Lab Invest 2008; 88:773-84; PMID:18490900; http://dx.doi.org/10.1038/labinvest.2008.40
42. Giovannetti E, van der Velde A, Funel N, Vasile E, Perrone V, Leon LG, De Lio N, Avan A, Caponi S, Pollina LE, et al. High-throughput microRNA (miRNAs) arrays unravel the prognostic role of MiR-211 in pancreatic cancer. PLoS One 2012; 7:e49145; PMID:23155457; http://dx.doi.org/10.1371/journal.pone.0049145
43. Funel N, Morelli M, Giovannetti E, Del Chiaro M, Pollina LE, Mosca F, Boggi U, Cavazzana A, Campani D. Loss of heterozygosity status of D9S105 marker is associated with downregulation of Krüppel-like factor 4 expression in pancreatic ductal adenocarcinoma and pancreatic intraepithelial lesions. Pancreatology 2011; 11:30-42; PMID:21412023; http://dx.doi.org/10.1159/000322990
44. Woodfield TB, Miot S, Martin I, van Blitterswijk CA, Riesle J. The regulation of expanded human nasal chondrocyte re-differentiation capacity by substrate composition and gas plasma surface modification. Biomaterials 2006; 27:1043-53; PMID:16125219; http://dx.doi.org/10.1016/j.biomaterials.2005.07.032